Arab J Sci Eng (2015) 40:901–913
DOI 10.1007/s13369-014-1538-0

RESEARCH ARTICLE - MECHANICAL ENGINEERING

Characterization of NiTi and NiTiCu Porous Shape Memory Alloys Prepared by Powder Metallurgy (Part I)

Alaa Abdulhasan Atiyah · Abdul-Raheem Kadhum Abid Ali · Nawal Mohammed Dawood

Received: 3 February 2014 / Accepted: 30 November 2014 / Published online: 25 December 2014

Abstract In this paper, the effect of compacting pressure (150–450 MPa) and copper (Cu) additions (2.5, 5, 7.5 and 10 wt%) on the microstructure and physical properties of NiTi-based shape memory alloys prepared by powder metallurgy is studied. Many characterization techniques were employed in this study such as X-ray diffraction method and scanning electron microscope. The chemical composition of the prepared alloys and microstructure was achieved by using scanning electron microscope equipped with EDS. Differential scanning calorimetric is utilized to measure the transformation temperature of the prepared alloys. Several physical tests such as particle size distribution measurements, density and porosity of green compacted samples and density and porosity after sintering are achieved. XRD test shows that the master sintered samples consist of three phases at room temperature: NiTi monoclinic phase, NiTi cubic phase and Ni_3Ti hexagonal phase. Furthermore, ($CuNi_2Ti$) intermetallic compound is appeared in the samples with 2.5, 5, 7.5 and 10 wt% of Cu. According to the results, it was found that compacting pressure has an essential effect on the decreases in porosity percentage and the results show that (Cu) additions increase porosity percentage in all weight percentages of additives.

Keywords NiTi porous alloys · Fabrication · Effect of Cu additions · Characterization

A. A. Atiyah (✉) · N. M. Dawood
Department of Materials Engineering, University of Technology, Baghdad, Iraq
e-mail: dralaadelta@gmail.com

A.-R. K. A. Ali
Materials Engineering College, University of Babylon, Babylon, Iraq

1 Introduction

Nickel–Titanium alloy near the equiatomic concentration is well known for its shape memory effect (SME). Due to its unique physical and mechanical properties like room temperature ductility, damping effect, erosion resistance and biocompatibility, this material can be used for numerous smart engineering and biomedical applications [1,2]. Recently, porous structure NiTi has attracted attention for the potential use in bone implants. Similar to the dense counterpart, the materials exhibit the SME, super elasticity, biocompatibility and good mechanical properties. The exceptional feature of porous structure is that it allows in growth of bone tissues [3,4] and favors bone osseointegration as well as transport of body fluids through open interconnected pores. The super elasticity of this biomaterial offers the possibility for certain in situ recovery of the implant shape after an injury to the implants or to the surrounding hard tissues. For long-term replacement of bone defects, nitinol offers the advantage of interfacial porosity as well as a permanent structural framework. Porous NiTi shape memory alloy has, for example, been considered as a promising biomedical material for orthopedics and bone implant surgeries in recent years. Furthermore, variation of the porosity by changing the production parameters results in adjustability of the NiTi elastic modulus for matching the human bone.

Various methods for producing conventional porous metals and alloys currently exist, including casting, metallic deposition and powder metallurgy [4]. Preparation and characterization of porous NiTi were studied through several experimental projects. In this way, Yun et al. [5] investigated, in 2000, the microstructure and stress–strain behavior of porous NiTi intermetallic compounds fabricated by powder sintering of Ni, Ti and/or TiH_2. It was found that the pores are small and well distributed in the present porous

NiTi alloys and that the phase constituent and stress–strain behavior of porous NiTi alloys are significantly influenced by the sintering conditions (sintering temperature and sintering time) and TiH_2 additions. In 2002, Lagoudas et. al. [6] used hot isostatic press (HIP) for fabrication of porous NiTi shape memory alloy from elemental Ni and Ti powders. They were successful to obtain and analyze porous NiTi alloy with different porosity levels and different mechanical properties. The authors used a micromechanical averaging model for modeling their behavior under compressive mechanical loading. The results from the model were compared to their experimental data.

At the same time, Bram et al. [7] used the promising PM routes hot isostatic pressing (HIP) and metal injection molding (MIM) for the fabrication of NiTi compacts. The authors measured the mechanical properties of (HIP) samples by tensile test at room temperature. The components from both fabrication routes show reversible austenite ↔ martensite transformations, which are a prerequisite for SMEs. In 2006, Bertheville [8] concluded that the synthesis of porous single-phase NiTi alloys by using a basic single-step sintering procedure is an important step toward the processing of safe implant materials. The sintering process used in this work is based on a vapor-phase calicothermic reduction operating during the NiTi compound formation. The as-processed porous nickel–titanium microstructure is single phase and shows a uniformly open pore distribution with porosity of about 53 % and pore diameters in the range 20–100 μm. Goryczka and Humbeeck [9] studied, in 2008, the sintering conditions (temperature and time) for the manufacturing of $Ni_{(50-X)}\,Ti_{50}\,Cu_X$ alloy (where $X = 5$, 10, 15, 20 and 25 at.%) by powder technology. Various conditions of sintering considering temperature and time were applied to compacted powders. The results showed that the homogenous alloys, containing lower addition of copper (<10 at.%), were sintered at 940 °C for 7 h, for higher copper content (10–25 at.%); lower sintering temperature 850 °C but longer sintering time was preferred (20 h).

In (2009), Sadrnezhaad and Hussein [10] successfully produced porous NiTi SMAs by using thermohydrogen process (THP). These processes have been able to produce a homogenous structure, appropriate pore-size distributions and short sintering times. The (THP) SMA samples produced in this research have a low Young's modulus of (19. 8 GPa) and high tensile strength of 255 MPa. These properties are close to those of the natural bone and can meet the mechanical property demands of the hard-tissue implants for heavy load-bearing applications. Lucaci et al. [11] studied, in 2011, the effects of addition, third alloy elements (Fe, Cu), to modify the phase transition temperature and the functional properties of NiTi alloy. They used powder metallurgy techniques to produce NiTi, NiTiFe and NiTiCu alloys. The results showed that the alloying elements contribute to the changing of the phase transformation temperature and of the functional properties of the materials, and the obtained materials are of multiphase type, consisting of NiTi, Ni_3Ti and Ni or Ni solid solution. It is found also after synthesis that only NiTiCu alloys exhibits a SME and NiTi and that NiTiFe alloys must be thermally treated in order to evidence the phase transformation.

In the present work, the powder metallurgy technique has been used to prepare porous NiTi shape memory alloys. Powder metallurgy techniques including conventional sintering, self-propagating high-temperature synthesis (SHS) and sintering at elevated pressure using a hot isostatic press (HIP) [12]. The primary advantage of powder metallurgy is the avoiding of typical thermomechanical treatment that is required after conventional casting. However, powder metallurgy produces pore which diminishes mechanical properties; this method which also enables easy production of complex-shaped parts has a controllable initial porosity ratio, lack of machining after production, display non-occurrence of segregation unlike the products obtained by casting method [9,13]. This paper aims to study the effect of compacting pressure and the Cu additives on the microstructure chemical composition and physical properties of NiTi shape memory alloys prepared by powder metallurgy.

2 Experimental Procedures

2.1 Compact and Alloy Preparation

The samples are prepared using powder metallurgy of NiTi powder, which consists of mixing, compacting and sintering processes. The purity, particle size and origins of powder used in this work are shown in Table 1. NiTi powder (master mixture, (55 wt% Ni with 45 wt% Ti) has been prepared using electric rolling mixer for 6 h. This mixture is used to prepare two groups, first, master alloy in four samples (without additive). Other samples are prepared with 2.5, 5, 7.5 and 10 wt% Cu. After mixing, cold uniaxial pressing in double action dies has been achieved. Electric hydraulic press with uniaxial pressing is used to compact green samples as disk samples with dimensions (14 mm diameter, 4 mm thickness) used for physical, differential scanning calorime-

Table 1 Purity %, average particle size and company of material

Material	Purity %	Average particle size (μm)	Company
Nickel powder	99.9	141.0–216.0	Bucks Fluka AG Co. Germany
Titanium powder	99.5	127.188	Fluke-Swiss
Copper powder	99.5	50.273	Strem Chemical, USA

Table 2 Detail description of prepared samples

Alloys	Sample code	Compacted pressure	Descriptions (wt%)
A	A1	150	55 % Ni + 45 % Ti
	A2	250	
	A3	350	
	A4	450	
B	B1	150	52.5 % Ni + 45 % Ti + 2.5 % Cu
	B2	250	
	B3	350	
	B4	450	
C	C1	150	50 % Ni + 45 % Ti + 5 % Cu
	C2	250	
	C3	350	
	C4	450	
D	D1	150	47.5 % Ni + 45 % Ti + 7.5 % Cu
	D2	250	
	D3	350	
	D4	450	
E	E1	150	45 % Ni + 45 % Ti + 10 % Cu
	E2	250	
	E3	350	
	E4	450	

ter (DSC) and microstructural tests. Four master samples each weighting 4 g are compacted at 150, 250, 350 and 450 MPa, respectively, by using a double action tool steel die with a diameter 14 mm. The same thing is done again with the samples containing 2.5, 5, 7.5 and 10 wt% Cu. Table 2 shows a description of prepared samples in detail. All samples were sintered at 850 °C for 9 h under controlled atmosphere of argon in pre-evacuated horizontal tube furnace (sintered samples with dimensions 14 mm diameter and 4 mm thickness).

2.2 Metallographic Preparation and Etching

All samples after sintering have been wet grinding using 180, 400, 800, 1,000, 1,200 and 2,000 grit silicon carbide papers. Then, samples polished with fine alumina type 0.03 μm fine polishing alumina. Etching was made at room temperature; for etching, 10 ml of hydrofluoric acid (HF), 20 ml of nitric acid (HNO_3) and 70 ml of water (H_2O) were used [14]. After washing with distilled water and dryer, this is stored in a desiccator for microstructure observation.

2.3 Porosity and Density

Despite the applied sintering technology, pores are inevitable components of the microstructure. They are classified as open—these ones, which have a contact with an outer surface of the compact—or closed ones—trapped space between particles. Their diameter mainly depends on particle size and compacting/sintering condition. The density of compacts (green density) was calculated from dimensions evaluations and weighting of compact sample as follows [15]:

$$\rho_g = \frac{m_g}{V_g} \tag{1}$$

where ρ_g = green density (g/cm^3), m_g = green mass of the compact (g) and V_g = volume of the compact (cm^3). The porosity of compacts (green porosity) is determined from theoretical density of blended powders (mixture), which is calculated by the weight percent of elemental powder multiplied by its theoretical density as follows [15]:

$$\rho_{tB} = \sum_{i=1}^{n} Wt_1 \times \rho_1 + Wt_2 \times \rho_2 + Wt_3 \times \rho_3 + \cdots + Wt_n \times \rho_n \tag{2}$$

where ρ_{tB} = theoretical density of blended powder (g/cm^3), n = No. of elemental powders, W_t = weight percent (%), $\rho_{1,2,3,\ldots,n}$ = density of elemental powder (g/cm^3). So the green porosity is calculated from the equation [15]:

$$P_g = \left(1 - \frac{\rho_g}{\rho_{tB}}\right) \times 100\,\% \tag{3}$$

where P_g = green porosity (%), ρ_g = green density (g/cm^3), ρ_{tB} = theoretical density of blended mixture (g/cm^3). The density and porosity of sintered part are calculated according to ASTM B-328 [16].

2.4 Experimental Methods

Diffraction particle size analyzer named SHIMADZU-SALD-2101 was applied to characterize the particle size distribution of the initial powders. The chemical composition of the prepared alloys was determined using an energy-dispersive system (EDS) attached to a scanning electron microscope (SEM, TM = 1,000 Hitachi table top—Japan made), which benefited to observe the microstructure of sintered alloys. In order to study thermal behavior of the martensitic transformation, DSC (A35 DSC—German made) was used. DSC samples cut by cutting wire machine (at the surrounding of sintered sample), which weighted 5 mg, were heated up to 120 °C and then cooled to −100 °C with cooling/heating rate of 10 °C/min. The cooling agent in the DSC test was liquid Nitrogen. The phase identification as well as structural parameters of the sintered samples was established using X-ray diffraction method. A Riga Ku X-ray generator with Cu K α radiation at 40 KV and 20 m A was

used. The X-ray is generated by general electrical diffractometer(Minifcex II, Rgaku-200 g—Japan made), operating at a scanning speed of 6° (2 θ) per minute. The detector was moved through an angle of 2 θ = 0°–100°.

3 Results and Discussion

3.1 Powder Characterization

Table 1 shows the particle size distribution of Ti, Ni and Cu powders, respectively. It is evident that the average size of the powder was around 127.188 μm for Ti, 141.0–216.0 μm and 50.273 μm for Ni and Cu, respectively. Different particle size ranges are preferred for good compacts and also for good properties of the final sintered products [17].

3.2 Porosity and Density

Green density for green compacted samples is shown in Fig. 1 with respect to compacting pressure, 150, 250, 350 and 450 MPa. In the first stage of compaction, powder particles are rearranged so that bridging alloys occurs in a randomly arranged stack of loose powder particles partially eliminated. In the second stage, elastic and plastic deformations of the particles have taken place. The third stage of compaction includes fracture of powder particles that have been embrittled through work hardening, under the applied stress increment. The density of compacts was calculated from the ratio of volume (V) and mass (m). Figure 2 shows the changes in the green density versus copper content. The green density is increased when copper content increased from 2.5 to 10 wt%; this increase in green density is likely due to the density of copper (8.95 g/cm^3) which slightly differs from nickel (8.90 g/cm^3); as a result, the theoretical density of NiTiCu alloys is also increased [9].

Green porosity, which is the complimentary of green density, is shown in Fig. 3 as a function of compacting pressure; with increasing of compacting pressure, the density of the powder mass increases because the total amount of porosity in the mass decreases; however, the pore size and pore distribution will change as well [18]. Green density varies from 3.781 to 5.099 g/cm^3 with the change of copper content as shown in Fig. 2; consequently, to the change of the density, the green porosity slightly increased with increase in the copper content, as shown in Fig. 4. This increase in green porosity has the lowest value for the alloy with lower content of copper [19]. The densities after sintering as a function of compacting pressure (150–450) MPa are shown in Fig. 5. The density after sintering is increased with increase in the compacting pressure; this increase in density is likely due to the shrinkage of original pores during sintering. With increasing sintering temperature or sintering time, the shrinkage of the original pores increases [20]. Density after sintering as a function of copper content is shown in Fig. 6. It has been shown that sintering independently of temperature and time

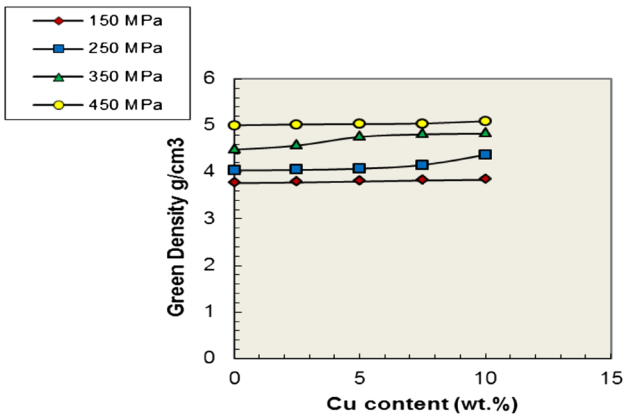

Fig. 2 Effect of copper content on the green density of alloys A, B, C, D and E compacted at different pressure

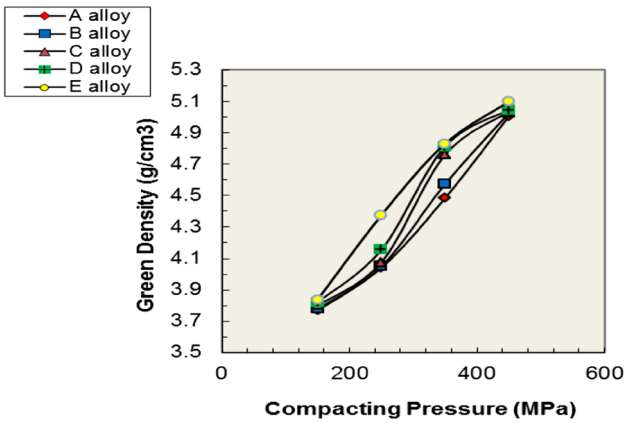

Fig. 1 Green density of alloys A, B, C, D and E with respect to compacting pressure

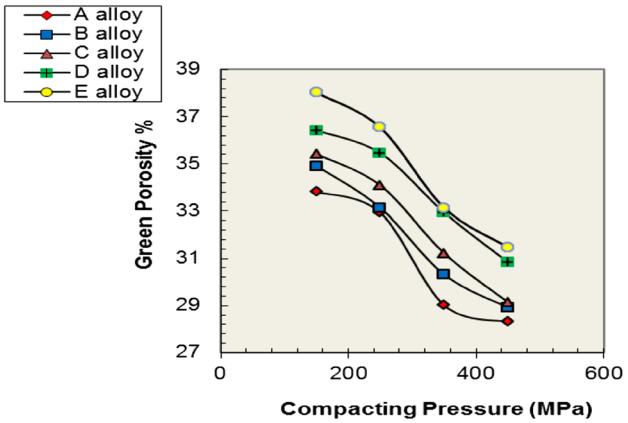

Fig. 3 Green porosity of alloys A, B, C, D and E with respect to compacting pressure

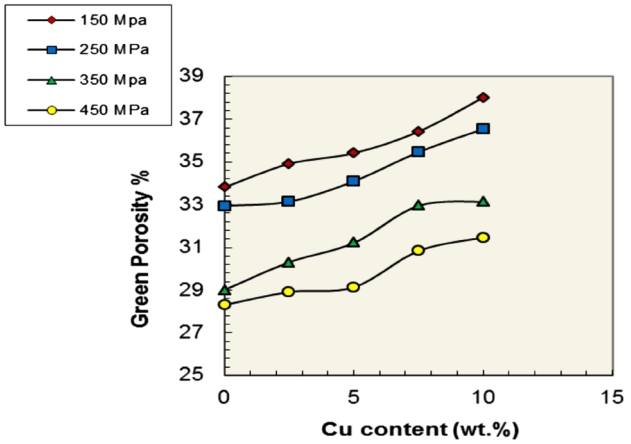

Fig. 4 Effect of copper content on the green porosity of alloys A, B, C, D and E compacted at different pressure

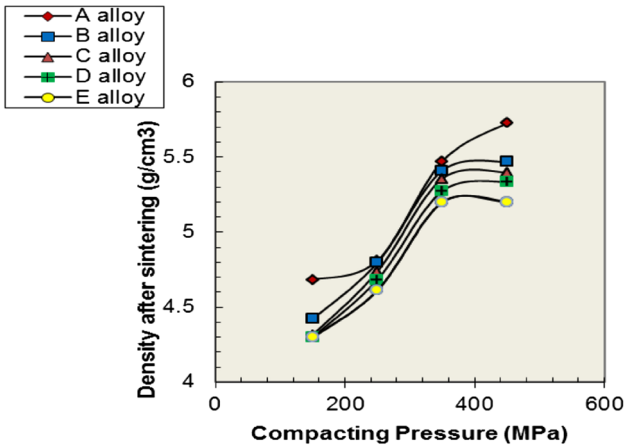

Fig. 5 Density after sintering of alloys A, B, C, D and E with respect to compacting pressure

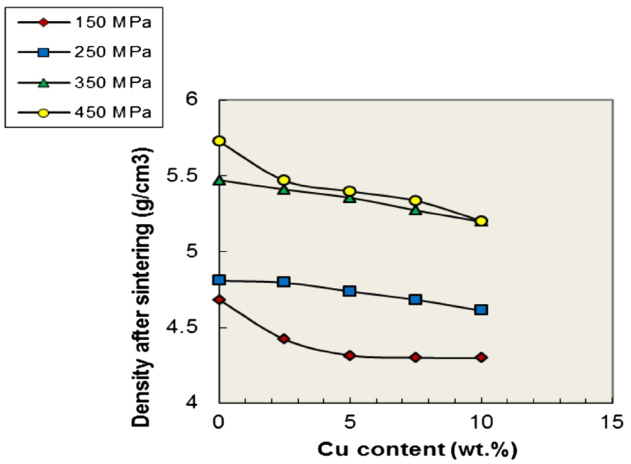

Fig. 6 Effect of copper content on the density after sintering of alloys A, B, C, D and E compacted at different pressure

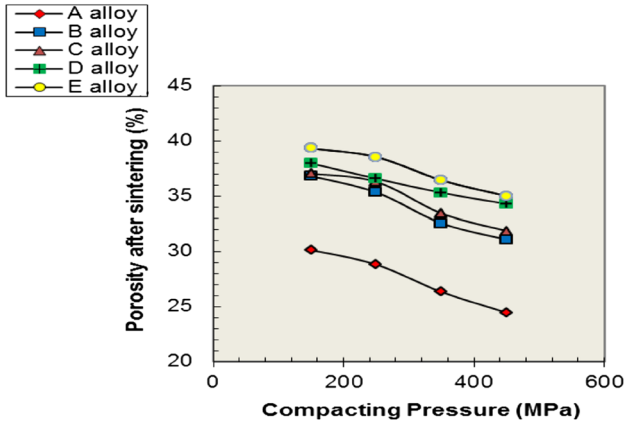

Fig. 7 Porosity after sintering as a function of compacting pressure for alloy alloys A, B, C, D and E

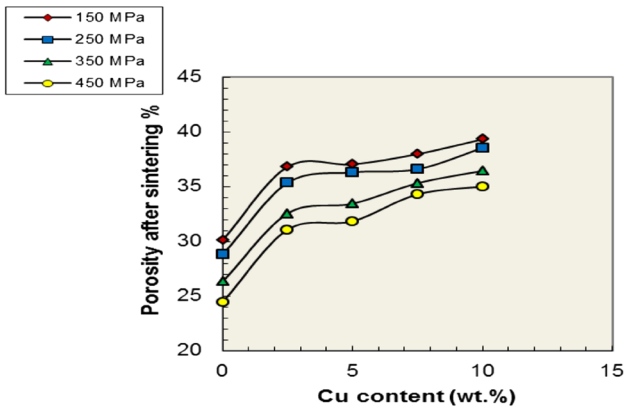

Fig. 8 Effect of copper content on the porosity after sintering of alloys A, B, C, D and E compacted at different pressure

results in a decrease in the density with increasing copper content as shown in Fig. 6 [9]. Porosity after sintering is the amount of open pores in the volume of sintered compact. Porosity after sintering as a function of compacting pressure is shown in Fig. 7. It has been shown that open pore volume fraction or porosity after sintering is deceased due to densification at high compacting pressure so that the pores are reduced [15,18].

On the other hand, porosity after sintering is increased when copper content is increased as can be seen from Fig. 8. This can be explained as follows: The diffusion of copper atoms in titanium is several times higher than diffusion of nickel atoms in titanium. Also, the diffusion ratio of copper and nickel atoms in titanium is higher than titanium in copper or nickel. As a consequence, titanium particles create a base for an alloy, where first copper atoms diffuse in and second nickel. In this manner, the volume of the pores increases. Using this mechanism, pores with smaller size can be created at the border between titanium particles and copper/nickel [19].

3.3 Chemical Composition Analysis

A preliminary scan for elements was conducted on the sintered samples (without copper and with different additives of copper) by using energy-dispersive spectrometer (EDS). The results are shown in Tables 3, 4, 5, 6 and 7 for A3, B3, C3, D3 and E3 samples, respectively. EDS technique was used to determine the mean value of chemical composition for micrograph of sample A3 (without copper addition); Table 3 shows the chemical composition of the A3 sample. In the present study, A3 sample were prepared to have 55 wt% Ni + 45 wt% Ti, which correspond to 55.72 wt% Ni and 44.28 wt% Ti in EDS results.

Tables 4, 5, 6 and 7 show no evidence of elements other than Ni, Ti and Cu, except sample B3 (which contains 2.5 wt% Cu). EDS results indicates that there are no element present other than Ni and Ti with the absence of copper element. These results may attribute to the characteristic of EDS analysis which does not cover the total area, only the spot where the electron stroke [13]. As can be seen, the results of EDS analysis were relatively close from the percentage of addition, because the values gained from EDS analysis do not cover the total area as mentioned early.

Table 3 Chemical composition for master sample (A3)

Element	Series	unn. c (wt%)	norm. c (wt%)	Atom. c (at.%)
Titanium	K series	35.46	44.28	49.35
Nickel	K series	44.62	55.72	50.65
Total	80.1 %			

Table 4 Chemical composition for sample (B3)

Element	Series	unn. c (wt%)	norm. c (wt%)	Atom. c (at.%)
Titanium	K series	33.79	42.72	47.76
Nickel	K series	45.32	57.28	52.24
Total	79.1 %			

Table 5 Chemical composition for sample (C3)

Element	Series	unn. c (wt%)	norm. c (wt%)	Atom. c (at.%)
Titanium	K series	49.95	50.26	55.51
Nickel	K series	45.44	45.72	41.16
Copper	K series	4.01	4.02	3.33
Total	99.4 %			

Table 6 Chemical composition for sample (D3)

Element	Series	unn. c (wt%)	norm. c (wt%)	Atom. c (at.%)
Titanium	K series	37.48	45.01	40.89
Nickel	K series	39.44	47.37	52.79
Copper	K series	6.34	7.62	6.32
Total	83.26 %			

Table 7 Chemical composition for sample (E3)

Element	Series	unn. c (wt%)	norm. c (wt%)	Atom. c (at.%)
Titanium	K series	40.16	43.37	43.79
Nickel	K series	44.24	47.78	48.71
Copper	K series	8.19	8.5	7.50
Total	92.59 %			

3.4 Morphology and Microstructure of the Sintered Samples

Morphology of the outer surface of sintered samples with different copper content is shown in Fig. 9a–e. Significant difference in pore size and their distribution can be observed for samples that vary in copper content, samples A1 without copper addition and with 2.5, 5, 7.5 and 10 wt% of copper addition for B1, C1, D1 and E1 samples, respectively. It can be seen that pores in sample A1 Fig. 9a are little, randomly distributed and rarely interconnected; also, pores have a regular shape: circular or elliptical. Completely different morphology is shown in Fig. 9b–e for B1,C1, D1 and E1 samples, which contained 2.5, 5, 7.5, 10 wt% of copper. However, these samples are sintered at the same condition (compacted at 150 MPa and sintered at 850 °C for 9 h); the pores have irregular shape, and in most cases, they are interconnected. These findings have an excellent matching with that reported in [9].

The micrograph gained from SEM for all samples surface (without copper and with different additives of copper) after being etched with the above mentioned etching solution is shown in Fig. 10a–e. The micrographs are taken with 5.00KX magnification as shown in figures. It is clear from SEM images for A1, B1, C1, D1 and E1 samples which were compacted at 150 MPa and sintered at 850 °C for 9 h that the etching reveals grained boundaries, which are easily confused with the grain boundaries and pores shape. Also, the martensitic formed in most samples, without copper A1 and with 2.5, 5, 7.5 and 10 wt% of copper additions which belong to B1, C1, D1 and E1, respectively, have a needle-shape grains which are clearly shown, especially in 7.5 and 10 wt% of copper additions. The needle-shape microstructure of martensite, which appeared in order pattern, is shown obviously in Fig. 10a, c, d, e which belong to A1, C1, D1 and E1 samples, respectively.

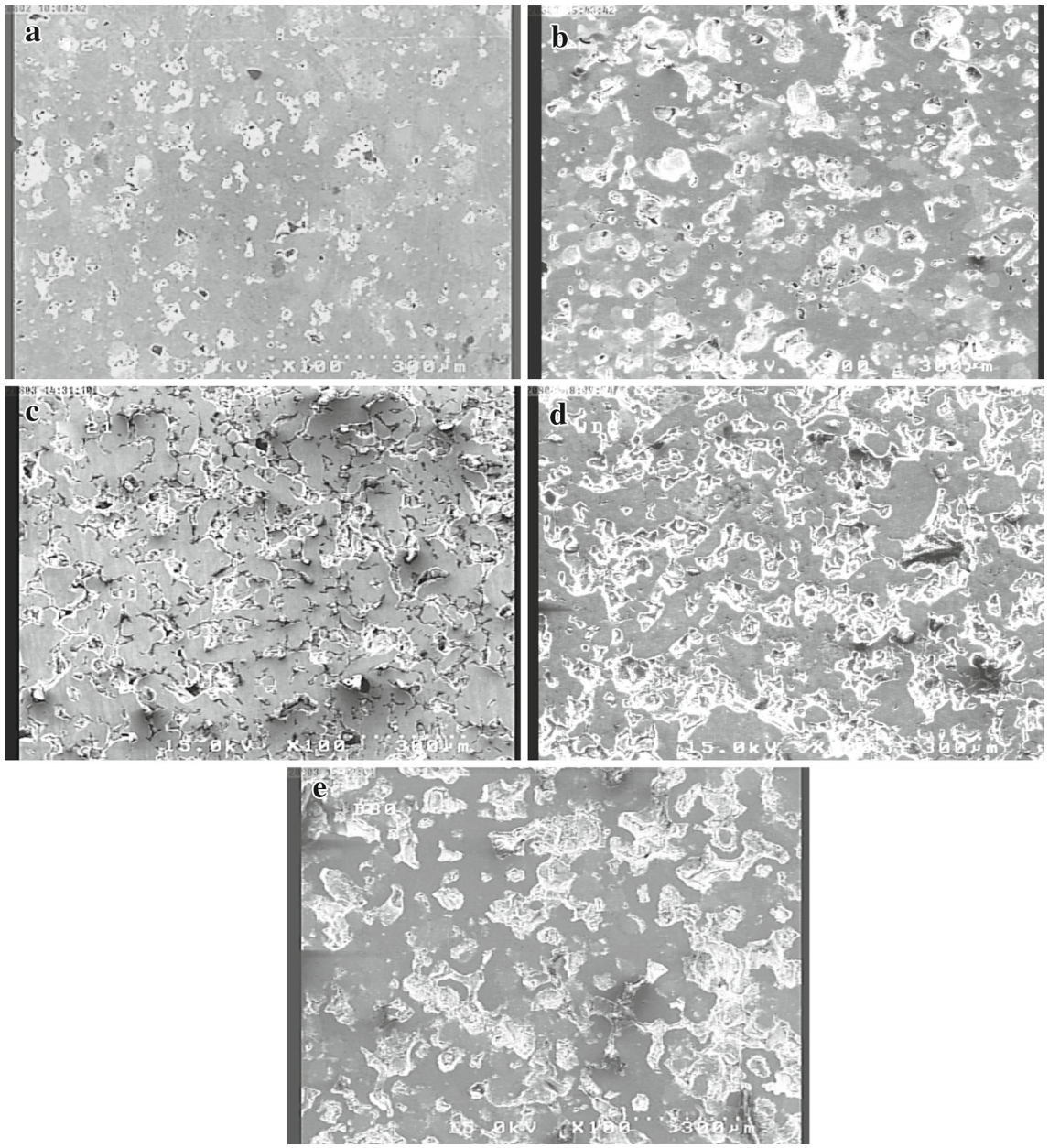

Fig. 9 SEM images showed the pore morphology in alloys A1, B1, C1,D1 and E1 with different content of copper at **a** 0 wt%, **b** 2.5 wt%, **c** 5 wt%, **d** 7.5 wt% and **e** 10 wt%, respectively

3.5 XRD Pattern

Figure 11a shows the XRD pattern for the sample A4 sintered at (850 °C for 9 h); it is clear from this figure that there are three phases NiTi monoclinic phase, NiTi cubic phase and Ni_3Ti hexagonal. The formation of Ni_3Ti might be attributed to the slow cooling of samples within the furnace; the suggested reactions during the process are as follows [5].

$$\mathbf{Ni + Ti \rightarrow NiTi} \quad \mathbf{\Delta G : -67}\ \text{KJ/mol} \tag{4}$$

$$\mathbf{Ni + Ti \rightarrow Ni_3Ti} \quad \mathbf{\Delta G : -140}\ \text{KJ/mol} \tag{5}$$

According to the binary phase diagram of NiTi system, NiTi and Ni_3Ti are stable compounds and reaction (5) is more thermodynamically favored than reaction (4). It is also found from Fig. 11a the absence of any oxides, which is attributed to the controlled argon atmosphere used during the sintering process. The significant decrease in Ni_3Ti hexagonal phase and strong increase in NiTi monoclinic phase lead to enhance the shape memory properties for the alloy. The results are similar to results in [18,21]. Figure 11b–e correspond to the B4, C4, D4 and E4 samples, respectively. These figures illustrate that there are no indication to the presence

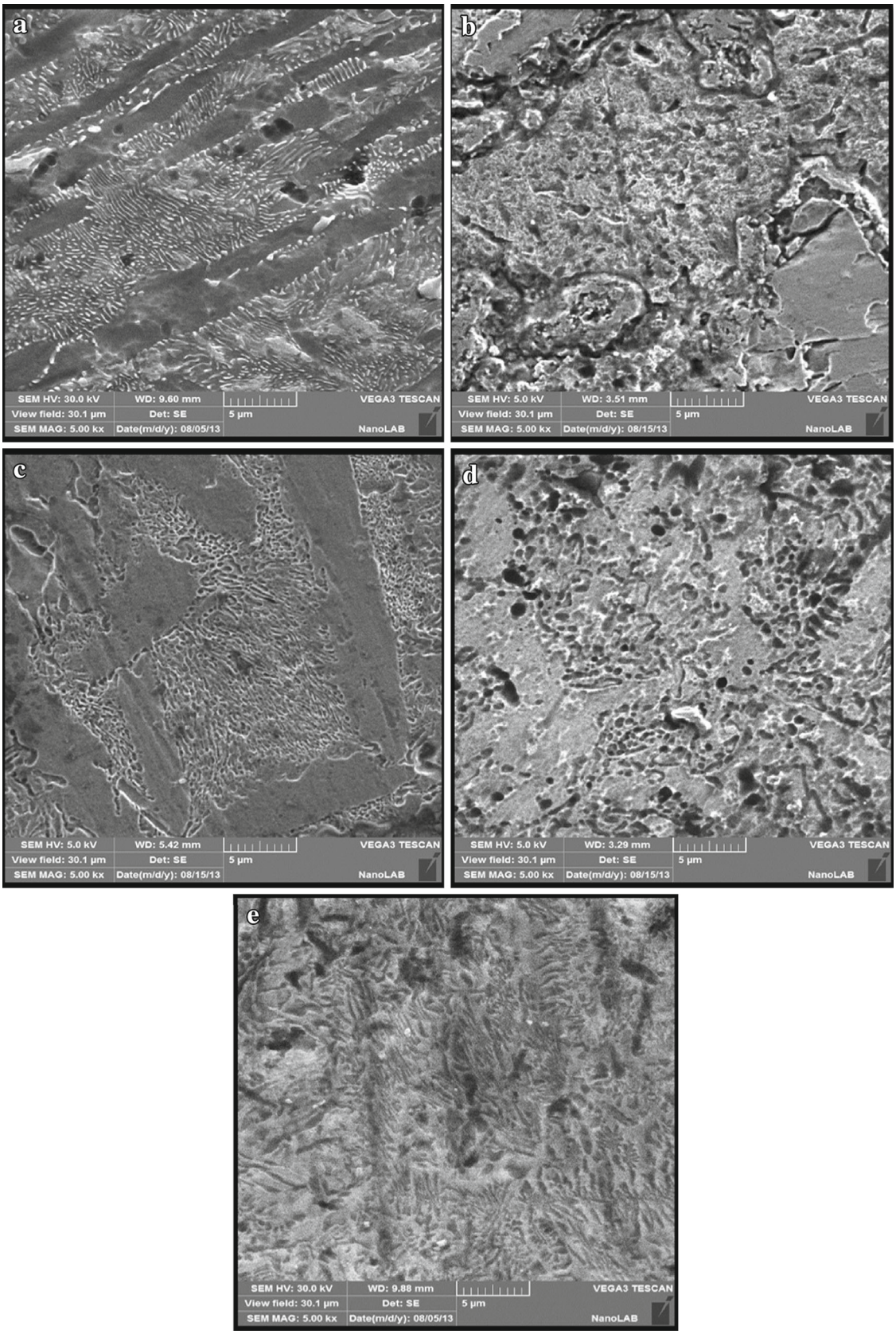

Fig. 10 SEM images for etched alloys A1, B1, C1, D1 and E1 with different content of Cu at **a** 0 wt%, **b** 2.5 wt%, **c** 5 wt%, **d** 7.5 wt% and **e** 10 wt%, respectively

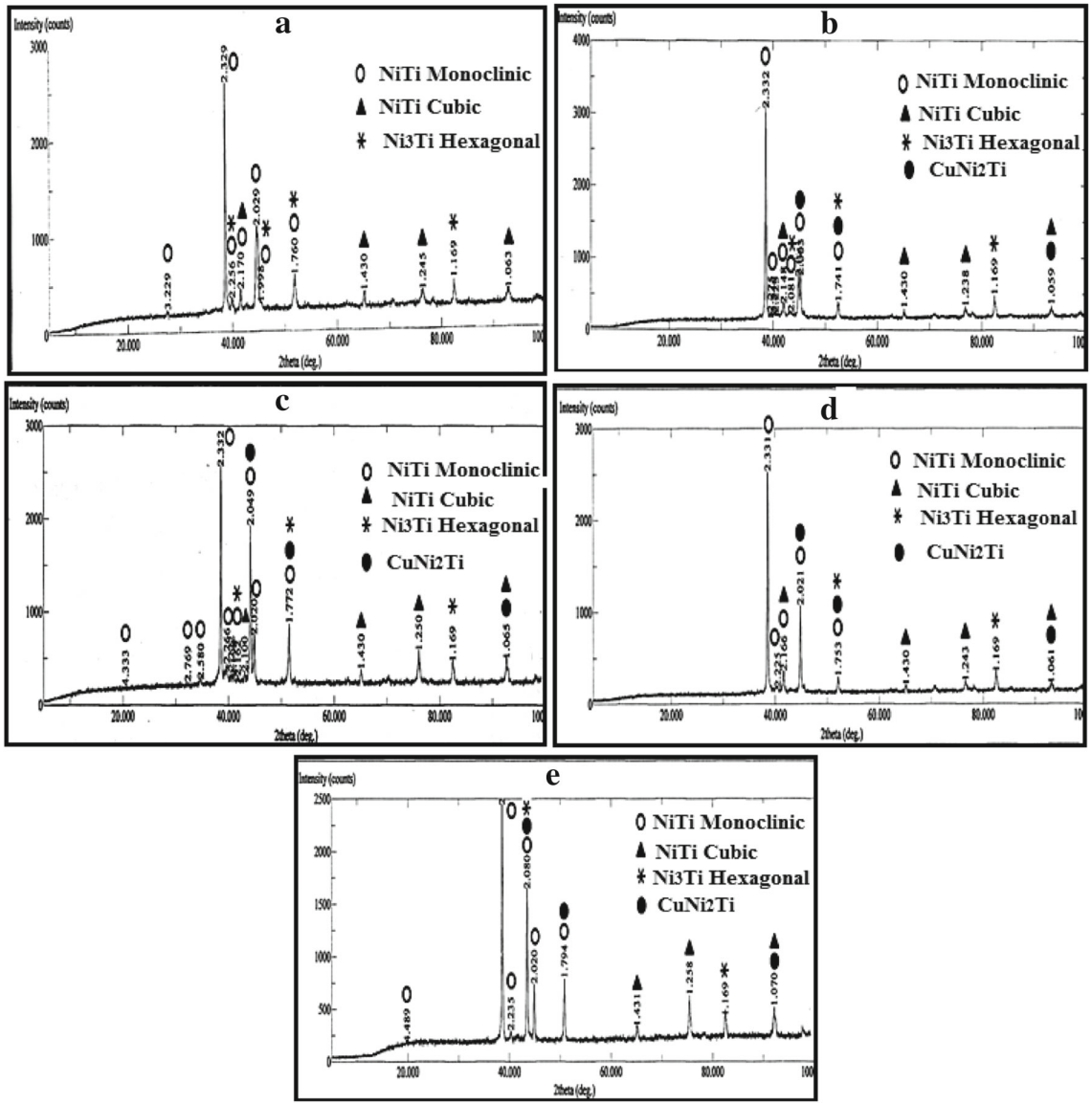

Fig. 11 X-ray diffraction analysis of the studied samples: **a** A4, **b** B4, **c** C4, **d** D4 and **e** E4 after sintering at 850 °C for 9 h

of any new phase other than NiTi monoclinic phase, NiTi cubic phase and Ni_3Ti hexagonal except $CuNi_2Ti$ intermetallic compounds as a result of copper additions.

3.6 Transformation Temperatures

The thermal scans presented in Fig. 12a–e proved the martensitic transformation in the prepared samples A3, B3, C3, D3, and E3, respectively. Analyzing Fig. 12a, it can be observed that the master alloy A3 during the heating cycle have two peaks at temperature 79.28–96.36 and 97.59–106.74 °C. They may be attributed to the two independent transformations or to the two-step transformation. While during cooling, the cooling cycle of the alloy from austenite to martensite has only one transformation, proved by one sharp peak; the single-step transformation indicates well-established B2 ↔ B19′. Figure 12b–e shows the samples with 2.5, 5, 7.5 and 10 wt% of Cu addition, respectively. As it can be seen, only NiTiCu alloys exhibits a one-step martensitic transformation on heating and cooling with a relatively wide DSC peak. One of the effects of copper addition in substation for nickel is the elimination of this R-phase intermediate transformation as can be verified from Fig. 12b–e, and this is in agreement with [19,22,23].

The values of phase transformation temperature of SMA essentially depend on a severe control of its chemical composition as well as of the mechanical forming manufacture processes. For instance in the literature, it is found, for equiatomic NiTi or near equiatomic NiTi SMA, the values of Ms, Mf, As and Af are obviously decreased with an addi-

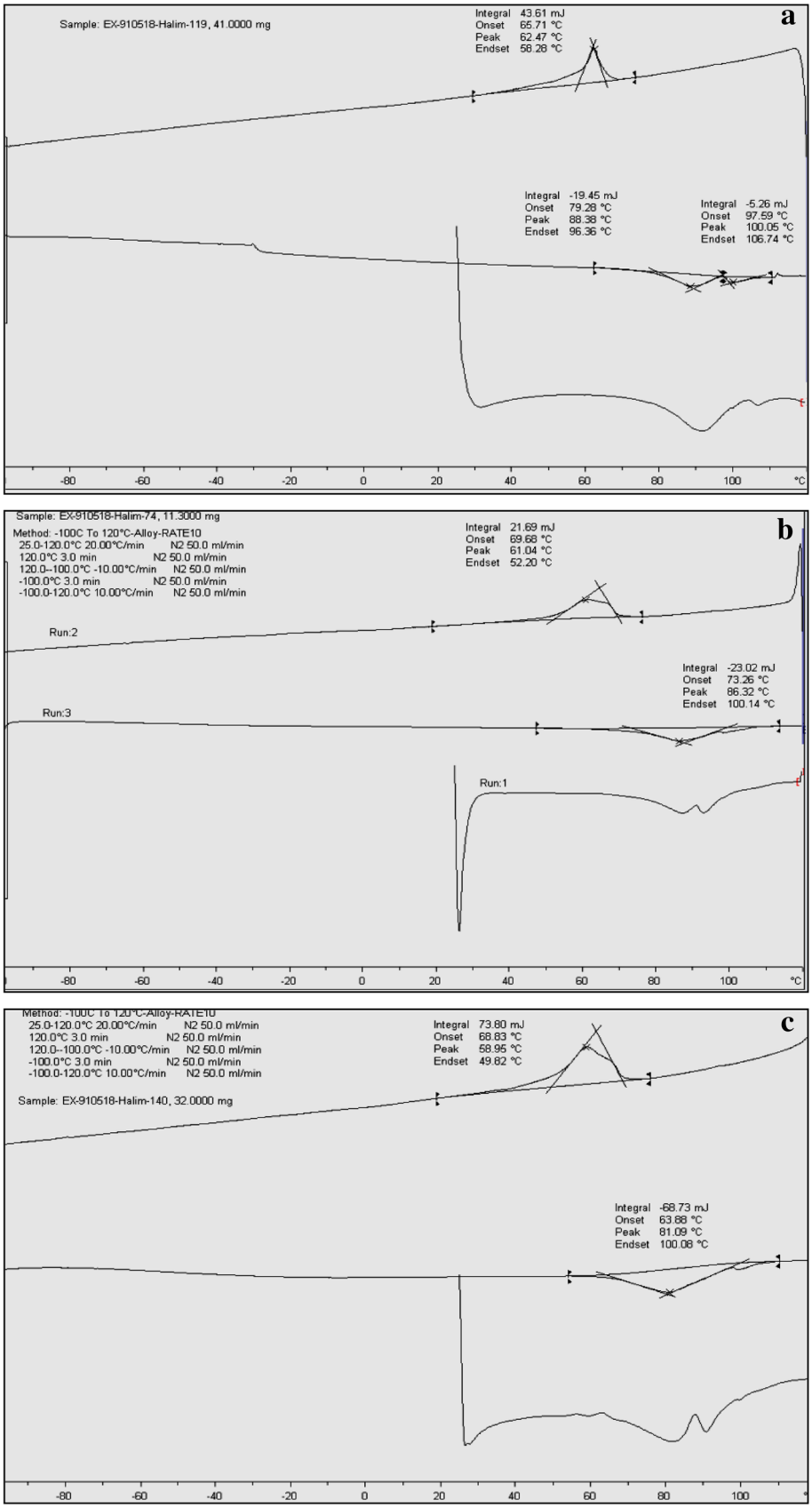

Fig. 12 DSC analysis showing phase transformation temperature of the studied SMA.**a** A3, **b** B3, **c** C3, **d** D3, **e** E3

Fig. 12 continued

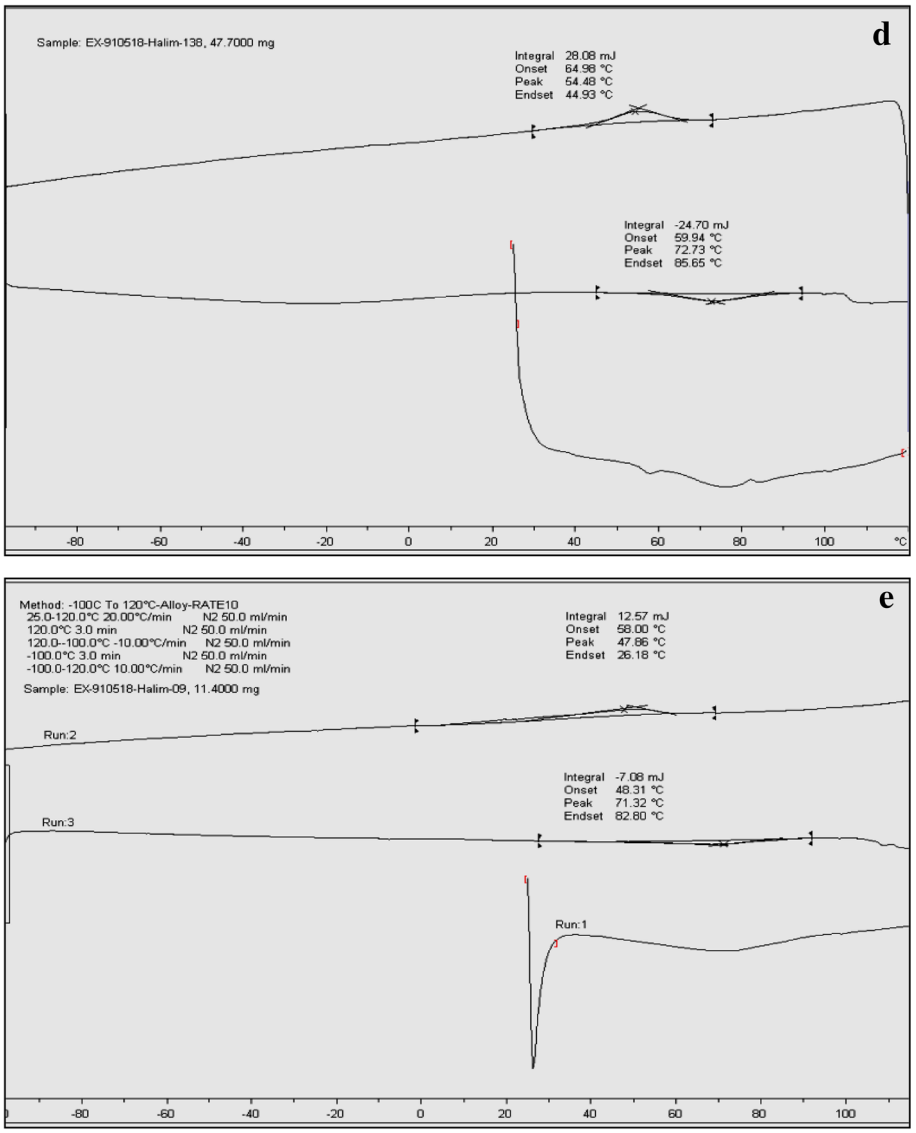

tion (5.6 wt%) of copper to NiTi alloys [24]. Figure 12b–e and Table 8 show that the phase transformation temperatures obtained for the studied NiTiCu SMA are in agreement with this literature, and any deviation is attributed to inaccurate compositional stoichiometry of the prepared samples. Copper addition to NiTi can raise the stability of the alloy during temperatures changes and mechanical loading. The mechanism for this effect is thought to involve inhibiting the nucleation and growth of both R-phase and Ni_4Ti_3 precipitate [22]. Figure 13a–d shows the changes in the transformation temperature Ms, Mf, As, Af as a function of copper content, respectively.

Table 8 Martensitic characteristic temperatures (Ms, Mf, As and Af), range of martensitic transformation (Af–Mf) and thermal hysteresis (Af–Ms)

Alloy	As (°C)	Af (°C)	Ms (°C)	Mf (°C)	Af–Ms Ht (°C)	Af–Mf (°C)
A3	79.28	96.36	65.71	58.28	30.65	38.08
B3	73.26	100.14	69.68	52.20	30.46	47.94
C3	63.88	100.08	68.83	49.82	31.25	50.26
D3	59.94	85.65	64.98	44.93	20.67	41.65
E3	48.31	82.80	58.00	26	24.80	56.8

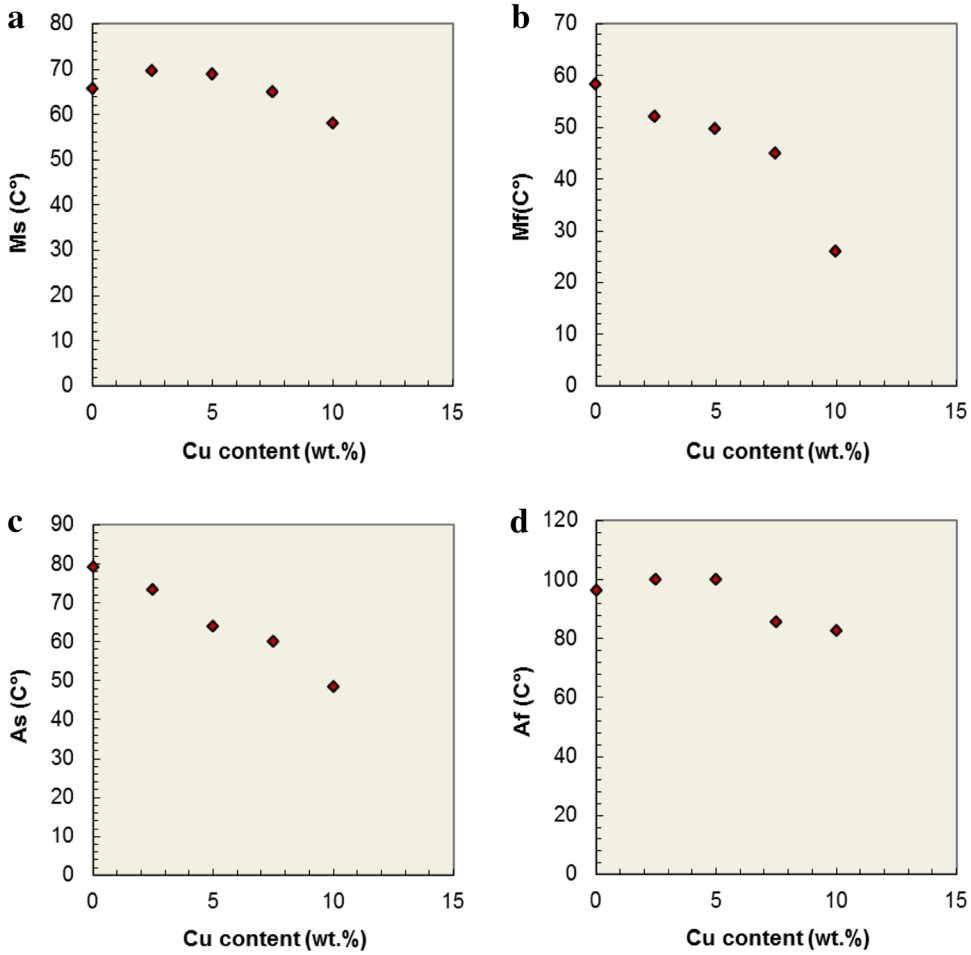

Fig. 13 Effect of copper content on **a** Ms, **b** Mf, **c** As and **d** Af temperatures (°C) for A3, B3, C3, D3 and E3 samples (pressed at 350 MPa and sintered at 850 °C for 9 h)

4 Conclusions

The porous NiTi and NiTiCu shape memory alloys have been successfully manufactured by powder technology. However, only a correct combination of sintering temperature and time leads to a homogeneous alloy. The following points can be concluded:

1. By the processing of SMA materials via powder metallurgy route, a special attention must be showed to the working atmosphere in order to sub-press the impurification with oxygen and carbon of the material.
2. The best sintering conditions for NiTi and NiTiCu alloys with different content of copper (2.5–10) wt% are 850 °C ± 5 for 9 h, which give a homogenous regularly transformed materials.
3. The master sample (without copper) compacted at 450 MPa and sintering at 850 °C ± 5 for 9 h resulted in a three-phase structure (NiTi monoclinic phase, NiTi cubic phase and hexagonal Ni_3Ti phase) at room temperature, while the samples with copper additions (2.5–10) wt% also resulted in the same three phases, furthermore, intermetallic compounds ($CuNi_2Ti$) at room temperature.
4. Copper addition to equiatomic NiTi alloy, in substitution for nickel, can modify the microstructure morphology of the alloy.
5. The addition of Cu with (2.5–10) wt% of NiTi prepared alloy resulted in an increasing the porosity as compared to the master alloy without copper.
6. From the DSC results with thermodynamic consideration; it was concluded that the martensitic transformation sequence B2 ↔ R ↔ B19′ was observed in NiTi alloys instead and that one-step martensitic transformation with sequence B2 ↔ B19′ was observed in NiTiCu alloys.
7. Another feature observed in NiTiCu alloy was the elimination of the intermediate R-phase transformation during cooling and heating, followed by a reduction in the thermal hysteresis. Thus, it was confirmed that the NiTiCu SMA are promising for applications as sensors and/or actuators where a faster activation frequency is important.

8. DSC results demonstrate that the values of Ms, Mf, As and Af of the master alloy obviously decrease with an addition (2.5–10 wt%) of copper.

Acknowledgments This work has been supported by Department of Materials Engineering at the University of Technology—Baghdad.

References

1. Tan, L.; Cron, W.C.: In situ TEM observation of two-step martensitic transformation in aged NiTi shape memory alloy. Scr. Mater. **50**, 819–823 (2004)
2. Pulletikurthi, C.; Munroe, N.; Gill, P.: Cytotoxicity of Ni from surface-treated porous nitinol (PNT) on osteoblast cells. J. Mater. Eng. Perform. **20**, 824–829 (2001)
3. Shabalorskaya: Surface corrosion and biocompatibility aspects of nitinol as an implant material. Bio-Med. Mater. Eng. **12**, 69–109 (2002)
4. Ryan, G.; Pandit, A.; Pan agiotis, D.: Fabrication methods of porous metals for use in orthopedic applications. Biomaterials **27**, 2651–2670 (2006)
5. Yun, B.; Jian, L.; Yili, Y.: Stress–strain behavior of porous Ni–Ti shape memory intermetallic synthesized from powder sintering. Intermetallic **8**, 643–646 (2000)
6. Lagoudas, D.; Entchev, P.; vandygriff, E.: The effect of transformation induced plasticity on the mechanical behavior of porous SMAs. Center for Mechanics of Composites, Aerospace Engineering Department (2002)
7. Bram, M.; Ahmad, A.; Heckerman, A.: Powder metallurgical fabrication processes for NiTi shape memory alloy parts. Mater. Sci. Eng. **A. 337**, 254–263 (2002)
8. Bertheville, B.: Porous single-phase NiTi processed under Ca reducing vapor for use as a bone graft substitute. Biomaterials **27**, 1246–1250 (2006)
9. Goryszka, T.; Humbeeck, J.V.: NiTi Cu shape memory alloy produced by powder technology. J. Alloy. Compd. **456**, 194–200 (2008)
10. Sadrnezhaad, S.; Hussein, S.: Fabrication of porous NiTi-shape memory alloy objects by partially hydride titanium powder for biomedical applications. Mater. Des. **30**, 4483–4487 (2009)
11. Lucaci, M.; Orban, R.L.; Tsakiris, V.: Shape memory alloys for MEMS components made by powder metallurgy processes. 2nd electronics system integration technology conference, Greenwich, UK (2011)
12. Randygriff, E.L.: Fabrication and characterization of porous NiTi shape memory alloy by elevated pressure sintering. M.Sc. Thesis, Texas, AZM University (2002)
13. Penrod, L.: Fabrication and characterization of porous shape memory alloys. M.Sc. Thesis, Texas, AZM University (2003)
14. Naresh, N.; Vreeland, T.; Ahrens, T.J.: Microstructural modifications in a dynamically consolidated microcrystalline nickel–titanium alloy powder. J. Mater. Sci. **22**, 4446–4452 (1987)
15. Kadhum, A. R.: Investigation of certain shape memory alloys in space system. Ph.D. Thesis, Department of Material Engineering, University of Babylon-Iraq, College of Engineering (2008)
16. ASTM B-328, Standard test method for density, oil content, and interconnected porosity of sintered metal structural parts and oil-impregnated bearing. ASTM International (2003)
17. Lakshmanan, A.: Sintering of ceramic—new emerging techniques. In Tech Web. Org. Croatia (2012)
18. Sadeq, M.A.: Corrosion behavior of biocompatible coatings of porous NiTi shape memory alloy. Ph.D. Thesis, Production Engineering and Metallurgy Department, University of Technology-Iraq (2013)
19. Goryczka, T.; Humbeeck, J.V.: Characterization of a NiTiCu shape memory alloy produced by powder technology. J. Achiev. Mater. Manuf. Eng. **17**(1-2), 65–68 (2006)
20. Li, B.Y.; Rong, L.J.; Li, Y.Y.: Porous NiTi alloy prepared from elemental powder sintering. J. Mater. Res. **13**(10), 2847–2851 (1998)
21. Otsuka, K.; Rin, X.: Physical metallurgy of Ti–Ni based shape memory alloys. Prog. Mater. Sci. **50**, 511–678 (2005)
22. Muir, A.J.; Sanjabi, S.; Fu, Y.Q.: Nano indentation of binary and ternary Ni–Ti-based shape memory alloy thin films. Surf. Coat. Technol. **202**, 3115–3120 (2008)
23. Valeanu, M.; Lucaci, M.; Crisan, A.D.: Martensitic transformation of Ti50Ni30Cu20 alloy prepared by powder metallurgy. J. Alloy. Compd. **509**, 4495–4498 (2011)
24. Deaujo, C.J.; Dasilva, N.J.; Dasilva, M.M.: A comparative study of Ni–Ti and Ni–Ti–Cu shape memory alloy processed by plasma melting and injection molding. Mater. Des. **32**, 4925–4930 (2011)